Laser Assisted Net Shape Engineering 5

Proceedings
of the 5th LANE 2007
Erlangen, September 25 - 28, 2007

Edited by M. Geiger, A. Otto, M. Schmidt
For CIRP, WGP and WLT

Volume 1

Meisenbach-Verlag Bamberg 2007

Die Deutsche Bibliothek – CIP-Einheitsaufnahme

Laser Assisted Net Shape Engineering 5
Proceedings of the 5th LANE 2007
Erlangen, September 25 - 28, 2007
ed. by M. Geiger, A. Otto, M. Schmidt
For CIRP, WGP and WLT.
Bamberg: Meisenbach, 2007
ISBN: 978-3-87525-261-3

Meisenbach GmbH, Franz-Ludwig-Straße 7a, D-96047 Bamberg

Layout: Bayerisches Laserzentrum & Lehrstuhl für Fertigungstechnologie
Print: Gruner Druck GmbH, Sonnenstraße 23, 91058 Erlangen

Laser Assisted Net Shape Engineering 5
Proceedings of the LANE 2007
Edited by: M. Geiger, A. Otto, M. Schmidt

NUMERICAL MODELLING OF THE THERMAL UPSETTING MECHANISM IN A TWO-BRIDGE ACTUATOR

J. Widłaszewski

Institute of Fundamental Technological Research of the Polish Academy of Sciences, Poland

Abstract

Angular deformation of the two-bridge actuator heated by a single laser pulse is analysed using finite element method. Experimentally validated numerical model allows deeper understanding of deformation mechanism, in particular the role of thermally generated bending load in the actuator. Prediction of laser-induced micro deformations requires determination of energy absorption and dissipation parameters with high accuracy. Experimental-numerical procedure was applied to find emissivity and coefficients of absorption and convection, using two-colour pyrometer and FEM simulations. The need for precise thermoplastic material data is demonstrated by means of a series of numerical simulations and the critical temperature concept.

Keywords: laser forming, two-bridge actuator, numerical modelling.

1 Introduction

Non-contact forming with the use of a laser beam has found many industrial applications in manufacturing of micro components. Thermal forming of big parts, e.g. ship hull plates, using different heat sources is under development with some successful implementations. Both areas of micro and macro thermal forming require thorough investigation of thermomechanics of the applied processes in order to possibly exactly model the involved phenomena and predict final shape and microstructural changes of the material. Behaviour of the two-bridge actuator [1], frequently applied in optoelectronic micro components, allows for effective studies of the role of modelling methods and material parameters in prediction of processing results.

Laser-induced deformations of the two-bridge actuator and other miniature frame structures have been investigated mainly experimentally [2], [3], [4], [5], [6], [7], but also modelled analytically [8], [9] and numerically [5], [10]. Presented research was primarily aimed at verification of theoretical assumptions employed in an analytical model for the behaviour of the two-bridge actuator presented at the previous LANE conference [9]. Efforts were concentrated on the basic phenomena and modelling aspects involved with thermally-induced micro deformations. Therefore experiments and simulations with the use of the finite element

method (FEM) were limited to a single pulse laser heating of a model structure (**Fig. 1**), deformation of which could be measured with sufficient precision, as presented in [9], [11]. Characteristic dimensions of the specimen made of the 18-8 type stainless steel (approx. 18% Ni, 8% Cr) were L = 6 mm, b = 10 mm, w = 2 mm and thickness h = 0.505 mm.

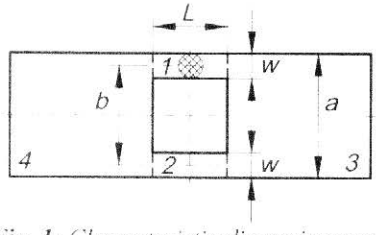

Fig. 1: Characteristic dimensions and notation of segments of the actuator.

2 Numerical model

Nonlinear uncoupled quasistatic analysis of thermo-elastic-plastic problem was conducted using the ABAQUS finite element method system. Taking advantage of the symmetry of the modelled sample and its thermal load only half of it was modelled (**Fig. 2**). Eight layers of finite elements on thickness of the material (**Fig. 7**) were employed to observe effects of the temperature gradient. The model contained 6016 solid 8-node linear full integration elements: DC3D8 for thermal analysis and C3D8 for stress/displacement analysis.

Multimode Nd:YAG laser beam was modelled as a heat flux of uniform distribution on the material surface. The nominal laser beam diameter was set up with the optical system to be equal to the width of the heated bridge.

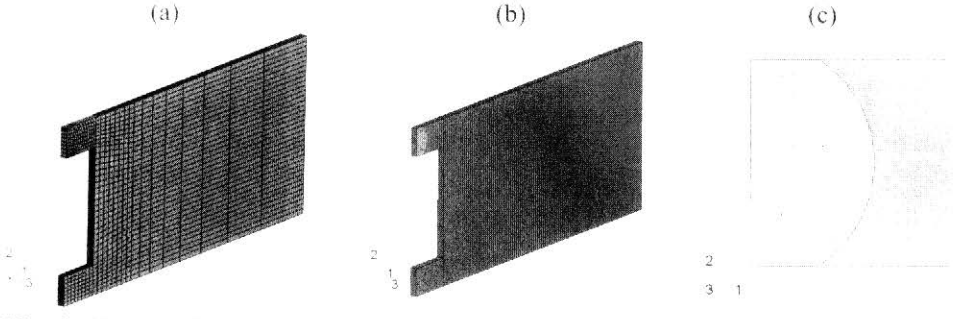

Fig. 2: Numerical model: (a) the applied mesh of elements on the half of the sample, (b) thermal load acting on one of the bridges, (c) laser spot region in detail.

However, due to existence of a trailing edge in the laser beam intensity distribution a part of the beam was not falling on the material surface and was going pass the sample. In the case

under consideration measurements of the laser radiation power behind the sample revealed that this fraction was about 8%. To account for this effect the laser spot diameter was assumed somewhat larger than the bridge width, as shown in **Fig. 2c**. The effectively applied laser beam power was corrected accordingly.

The applied temperature dependent data of the 18-8 type stainless steel are presented in **Figs. 3a-d**. Special attention has been given to two issues related to modelling of laser-induced plastic deformations, namely: (1) parameters of absorption and dissipation of the laser beam energy by the material, and (2) the sensitivity of modelling results to temperature dependence of the material yield stress.

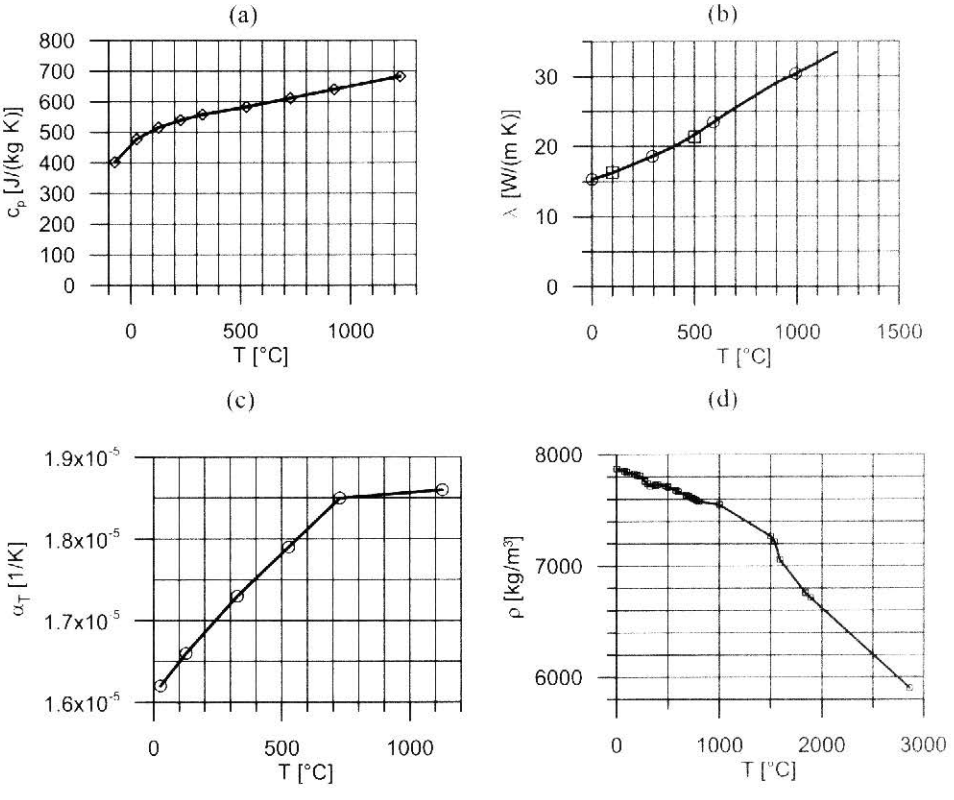

Fig. 3: *Thermophysical properties of the 18-8 type stainless steels: (a) specific heat c_p, (b) heat conductivity λ, (c) coefficient of linear thermal expansion α_T, (d) density ρ.*

Value of the laser beam energy absorption coefficient and value of the convection coefficient according to the Newton's law were established using experimental-numerical procedure. A square sample of dimensions 12 x 12 x 0.5 mm, made of the same stainless steel from which the two-bridge actuator samples were prepared, was irradiated by the Nd:YAG laser beam. The sample was annealed in a furnace for half an hour before laser irradiation experiments. The resulting oxide-film ensured stable absorption conditions for the laser heating experiments.

Temperature of the material during laser heating was measured by a non-contact method with a two-colour pyrometer Raytek FR1A CF1. In order to eliminate disturbance caused by the reflected radiation temperature measurements were conducted on the surface opposite to the surface irradiated with the laser beam. Recorded time-runs of the temperature during heating with the laser beam of different power levels and during subsequent free cooling were treated as reference data for numerical simulations of the same problem using the ABAQUS finite element method program.

Within the material temperature range of 500÷1100 °C relatively good agreement of the experimental and calculated temperature time-runs were obtained assuming the value of the absorption coefficient 0.92 and the value of the convection coefficient $4 \cdot 10^{-5}$ W/(°C cm^2). According to the Kirchhoff's law the material emissivity is equal to the absorption coefficient for the same radiation wavelength and in the same temperature.

The dependence of the material yield stress on temperature plays important role in modelling of elevated- and high-temperature plastic deformation processes like hot working and welding. Special difficulties arise when dealing with micro deformations involved in the laser adjustment method. High-temperature yield stress data usually come from hot compression or hot torsion tests and are based on a relatively high offset value, not adequate for micro adjustment processes. The strain rate sensitivity adds another factor to the complexity of the problem. **Fig. 4** presents some examples of the high-temperature yield stress data available in literature [12], [13], [14] for stainless steels of 18-8 type (e.g. AISI 304).

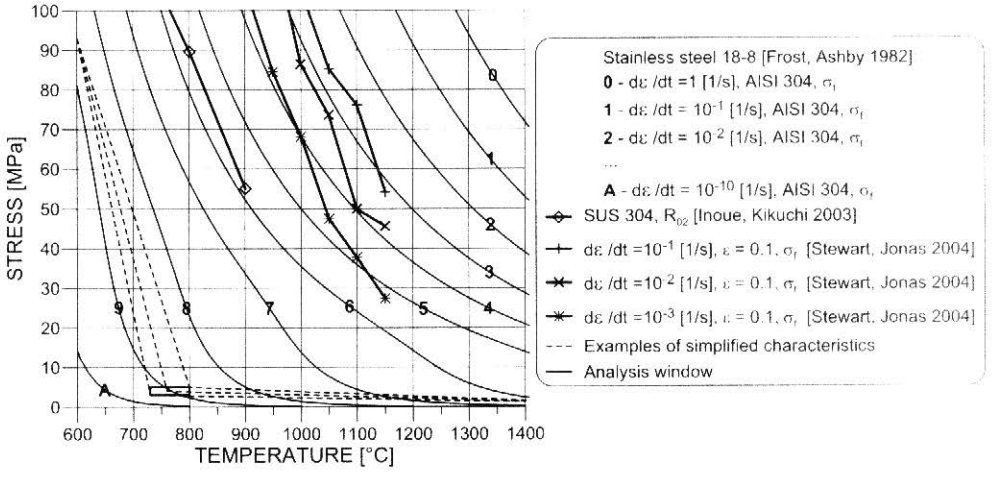

Fig. 4: *Examples of high-temperature yield stress data of the 18-8 type stainless steels.*

The figure contains curves calculated with an algorithm presented by Frost and Ashby [12] in their work on maps of deformation-mechanisms. The curves describe the steady state flow stress σ_f dependent on temperature and on the strain rate $\dot{\varepsilon} \equiv d\varepsilon / dt$ within the range $10^{-10} \div 1$ [1/s]. The assumed grain size of the steel is 50 microns.

Commonly employed method in modelling high-temperature deformations consist in application of the critical (cut-off) temperature concept [15], [16], [17]. It is successfully applied since introduction probably by Okerblom in his works on welding distortions [18], [19]. This approach relies in essence on the assumption that above certain temperature the material yield stress value can be neglected.

Similar method has been applied in currently presented work. Two points were added to the temperature-yield stress data [20] of the BS304S15 stainless steel: (1) the so called characteristic point of critical temperature T_{pl}, at which the yield stress assumes negligibly small value σ_{pl}^{cr} and (2) an auxiliary point of temperature 1500°C and yield stress 1 MPa added to avoid numerical instability of the FEM code. A few examples of material characteristics employed in simulations are marked by dashed lines in **Fig. 4**.

The Huber-Mises-Hencky yield criterion was applied together with a model of isotropic and elastic-perfectly plastic material, as strain hardening effect can often be neglected in high-temperature plasticity.

2 Experimental verification

The specimen was made from the 18-8 type austenitic stainless steel by laser cutting. It was annealed in a furnace for half an hour at 500°C in order to reduce residual stresses and to create oxide layer increasing and stabilizing absorption of laser radiation. One of the bridges (segment 1 in **Fig. 1**) was heated with Nd:YAG laser beam of 21.5 W power for 1.3 s. Angular deformation of the sample during laser heating and free cooling was measured in a non-contact manner with a laser scan micrometer (**Fig. 5a**) [9].

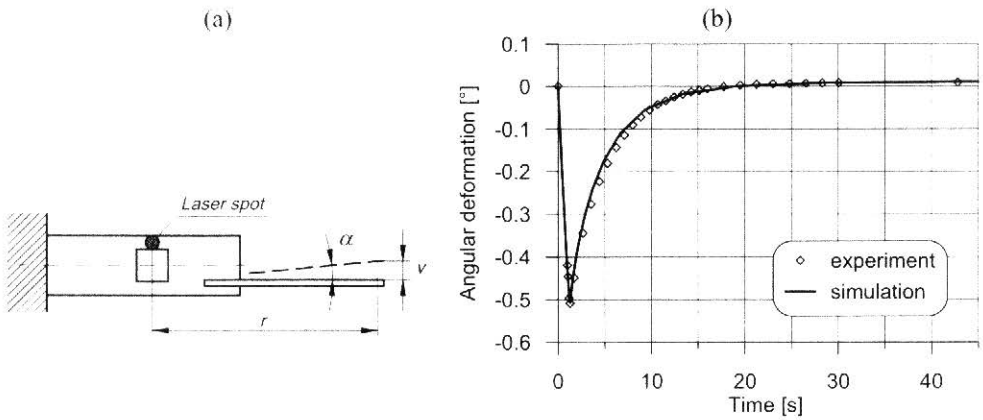

Fig. 5: *Experimental verification of the FEM model: (a) non-contact measurement of the angular deformation* α *, (b) comparison of experimental and numerical results.*

Time runs of the angular deformation of the specimen measured in experiment and calculated with FEM modelling are shown in **Fig. 5b**. Final angular deformation was 0.01°. The simulation was performed with the critical point parameters $T_{pl} = 840$ °C and $\sigma_{pl}^{cr} = 5$ MPa.

3 Discussion of results

The distribution of temperature at the end of laser heating phase (**Fig. 6**) justifies the Saint Venant's principle for the heat conduction problems. When material temperature reaches the highest value, its distribution is close to that of the one-dimensional heat transfer model, with the exception of some region near to the heat source.

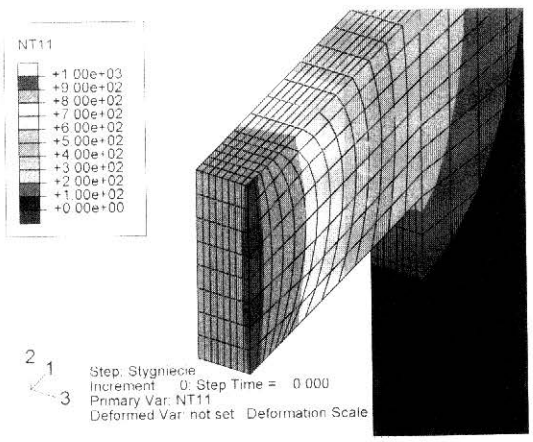

Fig. 6: The distribution of temperature [°C] in the segment 1 at the end of heating phase.

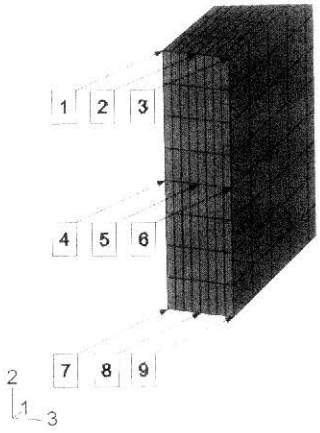

Fig. 7: Notation of points on the middle cross sections of segments 1 and 2.

Behaviour of the structure can be illustrated by thermal cycles of the stress and strain on the middle cross section of the heated segment 1. Changes of the axial (normal) stress component σ_{11} and the plastic strain component ε_{11}^{pl} during laser heating and free cooling are shown in **Figs. 8** and **9**, respectively. Notation of axes and points of analysis are presented in **Fig. 7**.

Thermal cycle of the axial stress component σ_{11} (**Fig. 8**) shows significant tension occurring at points 1-3 in segment 1 during the phase of heating, although the driving force for deformation of the actuator is thermal expansion of segment 1. Tensile internal forces result from a bending moment generated in the segment due to reaction and deformation of the whole structure. Only when material temperature approaches the maximal values at the considered locations (800-900°C), compressive forces become dominant on the bridge cross section. Together with decreasing yield stress, this leads to thermal upsetting of the segment in a form of a plastic collapse in its central region.

Thermal cycle of the longitudinal plastic strain component ε_{11}^{pl} (**Fig. 9**) reveals that dependent on the maximal temperature of the cycle, a part of the heated segment can end up the deformation process with positive (tensional) plastic strain (e.g. points 2 and 3).

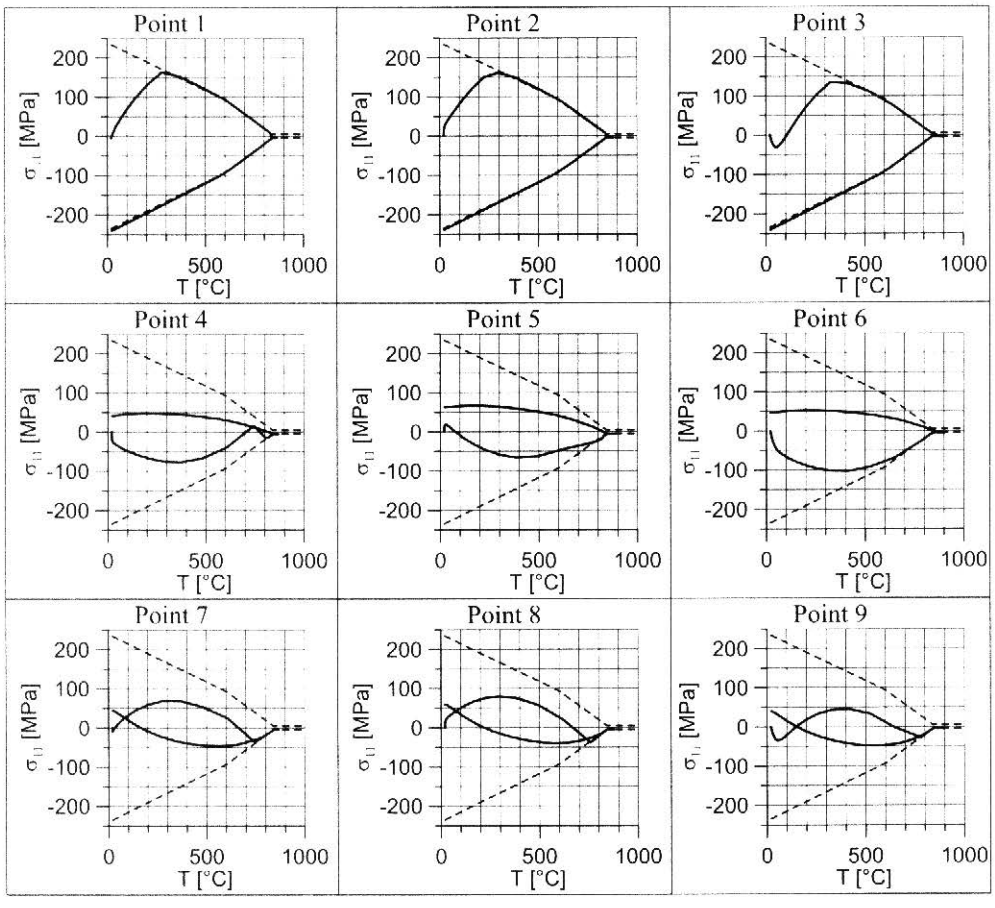

***Fig. 8**: Thermal cycle of the stress component σ_{11} at points 1-9 in segment 1. The dashed line denotes the applied yield stress dependence on temperature T.*

Comparison of graphs located in the same row (points 1-2-3, 4-5-6 or 7-8-9) in **Fig. 9** shows small effect of the temperature gradient on the actuator thickness. Time runs of the stress σ_{11} at points 2, 5 and 8 in segment 2 (**Fig. 10**) indicate strong bending with some small contribution of an axial load produced by deformation of the heated segment 1. After return to the initial temperature residual stresses in segment 2 result from the existence of the bending moment and a compressive force.

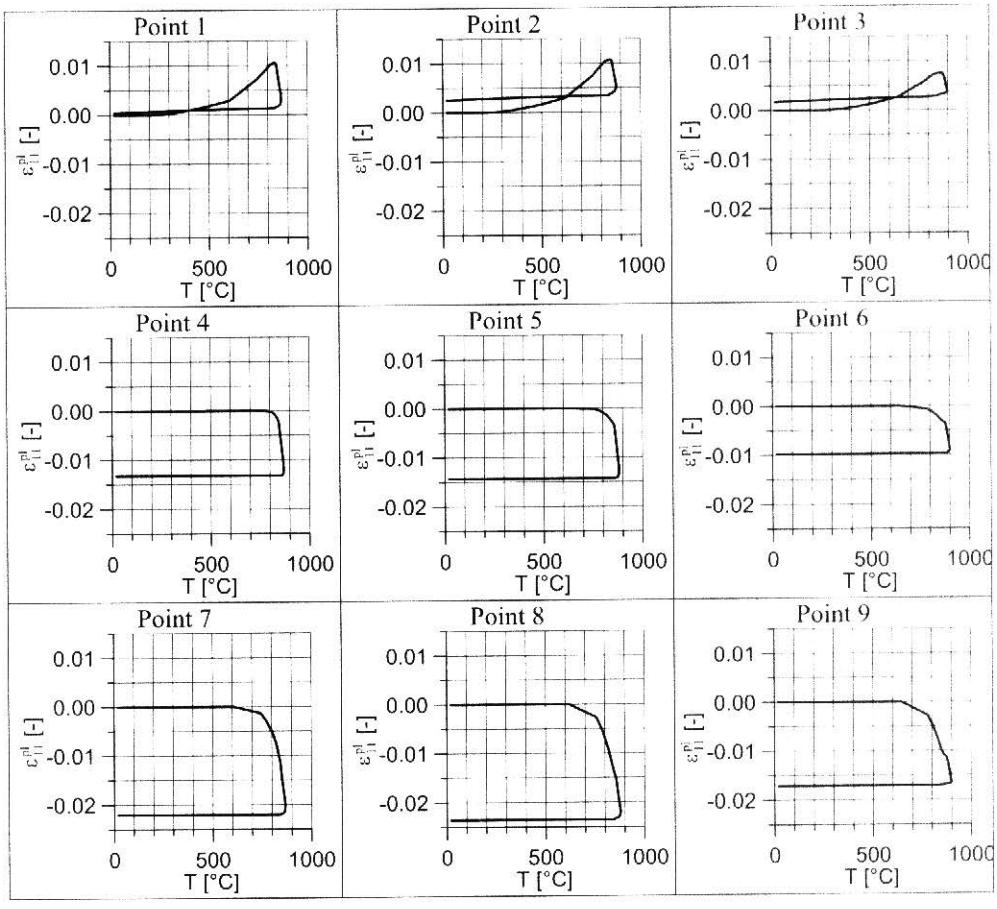

Fig. 9: *Thermal cycles of the longitudinal plastic strain component ε_{11}^{pl} at points 1-9 in segment 1.*

Time-runs of the normal stress component σ_{11} at points 1, 2 and 3 of segment 2 (**Fig. 11**) demonstrate the effect of temperature gradient during phase of heating.

Figs. 12a and **b** present comparison of the mean axial stress $\bar{\sigma}_{11}$ calculated from the resultant axial force in the heated segment 1, stress σ_{11} at the central point 5 of segment 1 and analytical solution presented in [9] during thermal cycle of heating and cooling.

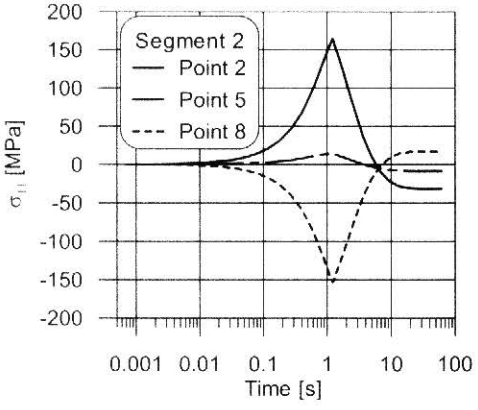

Fig. 10: Changes of stress σ_{11} at points 2, 5 and 8 of segment 2.

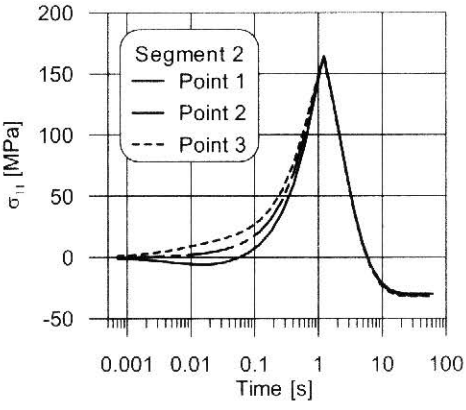

Fig. 11: Influence of the temperature gradient on stress σ_{11} in segment 2.

The courses of the mean axial stress $\overline{\sigma}_{11}$ and that of the stress σ_{11} at the central point 5 of segment 1 significantly differ from each other. However, the analytical solution during heating phase closely follows the mean axial stress $\overline{\sigma}_{11}$ course, what explains relatively good agreement of analytical and experimental results in [9] and [11].

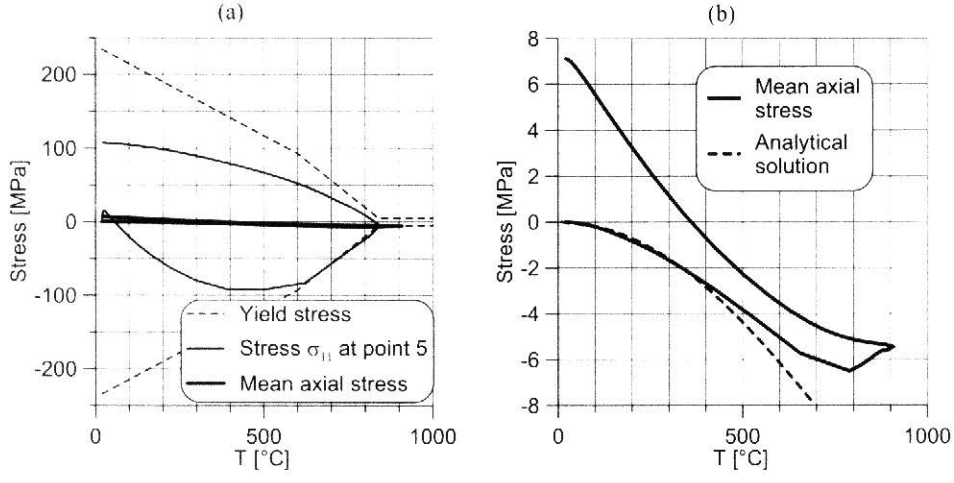

Fig. 12: Thermal cycle of the mean axial stress $\overline{\sigma}_{11}$, stress σ_{11} at the central point 5 of segment 1 and analytical solution: (a) FEM modelling results, (b) detailed view of the FEM modelling and analytical results.

Sensitivity of simulation results to the yield stress dependence on temperature can be illustrated by a diagram shown in **Fig. 13**. An experiment of heating the actuator with a Nd:YAG laser beam of power 16.7 W for 1.6 s was modelled in a series of simulations, using different yield stress simplified characteristics. The assumed critical temperature T_{pl} values were 730, 740, 750, 760, 770, 780, 790 and 800°C. The assumed yield stress σ_{pl}^{cr} values at the critical temperature were 3, 3.5, 4, 4.5 and 5 MPa. Results of altogether 40 simulations are presented in **Fig. 13** as a map of calculated permanent angular deformation α dependent on parameters T_{pl} and σ_{pl}^{cr}. Bold line denotes loci of solutions corresponding to the experimental result of 0.001° (0.017 mrad).

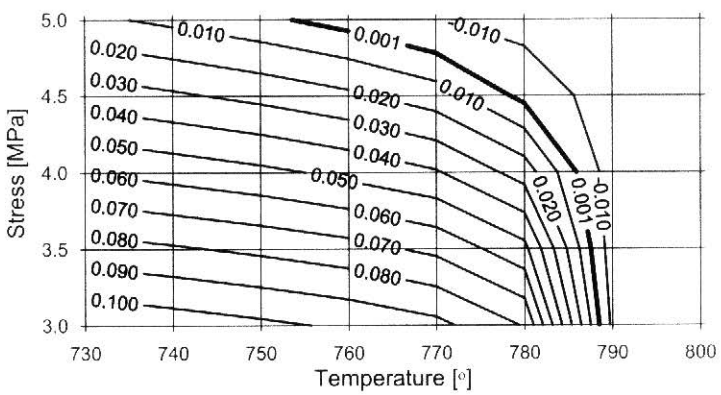

Fig. 13: *Map of permanent angular deformation of the two-bridge actuator calculated in FEM simulations using different parameters of critical temperature T_{pl} and stress σ_{pl}^{cr}.*

The map clearly shows high sensitivity of simulation results to thermoplastic material data, especially in modelling of thermally-induced micro deformations. A few percent change in the critical temperature T_{pl} value can give a change of the FEM result described by a factor of 100. Calculations performed on a personal computer with 2.6 GHz processor frequency and 1 GB RAM capacity took approximately 31 hours.

4 Conlusions

Numerical modelling of the two-bridge actuator allowed insight into thermomechanics of laser-induced plastic deformation of the structure. Apart from the upsetting mechanism, the behaviour of the actuator is influenced also by bending moments usually related to frame structures. The upsetting mechanism dominates high-temperature deformation of the actuator. Temperature gradient mechanism on the material thickness plays minor role in the case under consideration, where relatively long laser pulses were applied.

Modelling of thermally-induced micro deformations requires adequately accurate material data, in particular regarding energy absorption, dissipation and the material thermoplastic properties. Series of FEM simulations showed high sensitivity of numerical results to the yield stress dependence on temperature. Application of the critical temperature concept and simplified yield stress characteristics, although frequently necessary due to the shortage of high-temperature thermo-mechanical data of materials, can lead to significant errors of calculated micro deformations.

Acknowledgement

This work was partly done within the framework of the research project No. N503 012 31/1668 funded by the Ministry of Sciences and Higher Education of Poland in 2006-2009.

References

[1] Koster M. P., Semmeling R. A. E. M., Method of mutually displacing at least two parts of an actuator, and actuator suitable for use in such a method. Patent BE1007436. Publication date 1995-06-13.

[2] Huber A., Müller B., Vollertsen F., A measuring device for small angles and displacements. Proceedings of LANE'97, M. Geiger, F. Vollertsen (eds.), Meisenbach-Verlag, Bamberg 1997, 325-330.

[3] Hoving W., Verhoeven E. C. M., High-precision micro-assembly using laser-adjustment. Laser in der Elektronikproduktion & Feinwerktechnik - LEF 2000. Geiger M., Otto A. (eds.), Meisenbach Bamberg, 2000, 165-174.

[4] Olowinsky A. M., Bosse L., Laser beam micro forming as a new adjustment technology using dedicated actuator structures. Smart Sensors, Actuators, and MEMS. Chiao J.-C., Varadan V. K., Cane C. (eds.), Proceedings of the SPIE, Volume 5116, 2003, 285-294.

[5] Schmidt M., Dirscherl M., Rank M., Zimmermann M., Laser micro adjustment - from new basic process knowledge to the application. Journal of Laser Applications, Vol. 19, No 2 (2007) 124-132.

[6] Ossowski A., Widłaszewski J., Laser control of frame microstructures. NATO Advanced Research Workshop SMART-98, *Smart Structures*, Holnicki-Szulc J., Rodellar J. (eds.), Kluwer Academic Publishers, 1999, 255-264.

[7] Widłaszewski J., Thermal deformation of multilevel spatial structures induced by laser pulses. Proceedings of the LANE 2001, eds.: M. Geiger, A. Otto, Meisenbach-Verlag Bamberg 2001, 569-574.

[8] Otto A., Fundamentals of laser beam adjusting in micro systems. Thermal Forming. Proceedings of the IWOTE'05 (1st International Workshop on Thermal Forming), Bremer Institute für angewandte Strahltechnik. Vollertsen F., Seefeld T. (eds.), BIAS Verlag, Bremen 2005, 83-92.

[9] Widłaszewski J., Modelling of actuators for adjustment with a laser beam. Proceedings of the LANE 2004 (Laser Assisted Net Shape Engineering 4) International Conference, Geiger M., Otto A. (eds.), Meisenbach-Verlag Bamberg 2004, Vol. 2, 1083-1094.

[10] Huber A., Müller B., Meyer-Pittroff F., Laserstrahljustieren als Innovation für die Montage von Mikrosystemen. Vollertsen F., Kleiner M. (eds.), Idee - Vision Innovation, Meisenbach, Bamberg, 2001, 275-286.

[11] Widłaszewski J., Micro Adjustment by Thermal Upsetting. Thermal Forming, Proceedings of the IWOTE'05. Vollertsen F., Seefeld T. (Eds.), Bremer Institute für angewandte Strahltechnik GmbH, 2005, 93-109.

[12] Frost H., Ashby M. F., Deformation-Mechanism Maps. The Plasticity and Creep of Metals and Ceramics. Pergamon Press 1982.

[13] Inoue Y., Kikuchi M., Present and Future Trends of Stainless Steel for Automotive Exhaust System. NIPPON STEEL TECHNICAL REPORT, No. 88, July 2003.

[14] Stewart G. R., Jonas J. J., Static and Dynamic Strain Aging at High Temperatures in 304 Stainless Steels. Iron and Steel Institute of Japan (ISIJ) International, Vol. 44 (2004), No. 7, 1263-1272.

[15] Watanabe M., Satoh K., Effect of Welding Conditions on the Shrinkage Distortion in Welded Structures. The Welding Journal, Welding Research Supplement 40 (1961) 8, 377-384.

[16] Tsai C. L., Kim D. S., Understanding residual stress and distortion in welds: an overview. Chapter 1 in "Processes and mechanisms of welding residual stress and distortion", Feng Z. (ed.). Woodhead Publishing Limited and CRC Press LLC, Cambridge, 2005.

[17] Mollicone P., Camilleri D., Gray T. G. F., Comlekci T, Simple thermo-elastic-plastic models for welding distortion simulation. Journal of Materials Processing Technology 176 (2006) 77-86.

[18] Okerblom N. O., Projektieren von Schweißkonstruktionen. Kubutsch, Leningrad 1934.

[19] Okerblom N. O., The Calculation of Deformations of Welded Metal Structures. Her Majesty's Stationery Office, London, 1958.

[20] Sędek P., Problemy naprężeń i odkształceń spawalniczych (Welding stress and distortion problems). Seria Inżynieria Materiałowa (Materials Engineering Series). Biuro Gamma, Warszawa 2000 (in Polish).